J Bioenerg Biomembr (2012) 44:101–115
DOI 10.1007/s10863-012-9416-5

Enhancement of hexokinase II inhibitor-induced apoptosis in hepatocellular carcinoma cells via augmenting ER stress and anti-angiogenesis by protein disulfide isomerase inhibition

Su Jong Yu · Jung-Hwan Yoon · Jong-In Yang · Eun Ju Cho · Min Sun Kwak · Eun Sun Jang · Jeong-Hoon Lee · Yoon Jun Kim · Hyo-Suk Lee · Chung Yong Kim

Received: 27 December 2011 / Accepted: 14 January 2012 / Published online: 15 February 2012

Abstract 3-bromopyruvate (3-BP), a hexokinase (HK) II inhibitor, promotes tumor cell death by inducing endoplasmic reticulum (ER) stress in human hepatocellular carcinoma (HCC) cell lines. Protein disulfide isomerase (PDI) is an essential folding catalyst and attenuates ER stress by folding the misfolded proteins. We examined if PDI is expressed in hypoxic HCC cells, and evaluated its inhibition potentiated HK II inhibitor-induced ER stress in hypoxic HCC cells. HCC apoptotic cell death was assessed by DAPI staining and apoptotic signaling pathways were explored by immunoblot analysis. An in vivo model of HCC was established in C3H mice intradermally with implanted MH134 cells. 3-BP with/without a PDI inhibitor (bacitracin) was subsequently administered. The anti-tumor efficacies were evaluated by measuring tumor volumes and quantifying apoptotic cells and microvessel densities (MVDs). HCC cells were found to express PDI in a hypoxia-inducible manner. The simultaneous treatment of bacitracin and 3-BP enhanced 3-BP-induced apoptosis. This enhancement was attributed to increased ER stress and JNK activation compared to the cells treated with just 3-BP. In an in vivo model of HCC, tumor growth was significantly suppressed in mice co-treated with bacitracin and 3-BP, and the percentages of apoptotic cells significantly increased and MVDs significantly decreased. These results demonstrated that PDI was induced in hypoxic HCC tissue and that PDI inhibition enhanced HK II inhibitor-induced anti-tumor efficacy synergistically via augmenting ER stress and anti-angiogenesis in vivo. Thus, blockage of PDI activity in combination with HK II inhibitor may be therapeutically useful in HCCs.

Keywords Hepatocellular carcinoma · Hypoxia · Hexokinase II · Protein disulfide isomerase · Apoptosis

Abbreviations

3-BP	3-bromopyruvate
HK	hexokinase
ER	endoplasmic reticulum
HCC	hepatocellular carcinoma
PDI	Protein disulfide isomerase
MVDs	microvessel densities
TACE	transarterial chemoembolization
HIF-1	hypoxia inducible factor-1
UPR	unfolded protein response
JNK	c-Jun N-terminal kinase
DAPI	4′,6-diamidino-2-phenylindole dihydrochloride
eIF2α	eukaryotic initiation factor 2α
NONMEM	nonlinear mixed effect modeling
H&E	Hematoxylin and eosin
AP	alkaline phosphatase
SD	standard deviations
PERK	PKR-related ER kinase

S. J. Yu · J.-H. Yoon (✉) · E. J. Cho · M. S. Kwak · E. S. Jang · J.-H. Lee · Y. J. Kim · H.-S. Lee · C. Y. Kim
Department of Internal Medicine and Liver Research Institute, Seoul National University College of Medicine, 101 Daehak-ro, Jongno-gu, Seoul 110-744, Republic of Korea
e-mail: yoonjh@snu.ac.kr

J.-I. Yang
Department of Internal Medicine and Healthcare Research Institute, Seoul National University Hospital, Healthcare System Gangnam Center, Seoul, South Korea

IRE1	inositol requiring enzyme-1
XBP-1	X-box binding protein-1
ATF	activating transcription factor
ECs	endothelial cells

Introduction

Hepatocellular carcinoma (HCC) is the fifth most common malignancy worldwide and the fourth leading cause of cancer-related deaths (Parkin et al. 1999; Di Bisceglie et al. 1988). HCCs are characteristically hypervascular and therefore, transarterial chemoembolization (TACE), in which the therapeutic effect is based on hypoxic or anoxic damage to the tumor cells, is one of the more favorable treatment options for unresectable HCCs. However, locally recurrent HCC nodules after TACE sometimes show significantly shorter doubling times than those in neighboring nodules (Tezuka et al. 2007). Moreover, HCCs sometimes show an infiltrating rather than a mass-forming growth pattern (Trevisani et al. 1993; Weinstein-Oppenheimer et al. 2001) and these advanced infiltrative HCCs seldom show hypervascularity, grow more rapidly, and have a poorer prognosis than the mass-forming hypervascular types. These findings suggest that hypoxia seems to activate signals that allow HCC cells to survive and proliferate in hypoxic conditions (Gwak et al. 2005).

In a hypoxic state, the glycolytic system substitutes for oxidative phosphorylation as a rescue pathway of generating adenosine triphosphate (Gwak et al. 2005). Many glycolytic enzymes and glucose transporters are induced by hypoxia inducible factor-1 (HIF-1) through the hypoxia response element in the promoter regions of the genes (Pastorekova et al. 2008). Among these, hexokinase (HK) is the first enzyme in this pathway and is essential for maintaining the high glycolytic phenotype (Bustamante et al. 1981). We previously demonstrated that hypoxia stimulates HCC cell growth by inducing HK II expression (Gwak et al. 2005) and inhibition of HK II in vivo exhibits an anti-tumor effect by inducing apoptosis (Kim et al. 2007).

Recently, it was reported that 3-bromopyruvate (3-BP), an HK II inhibitor, may induce endoplasmic reticulum (ER) stress, disruption of the ER function, by the accumulation of free radicals or reactive oxygen species and the protein misfolding (e.g. GAPDH) (Ganapathy-Kanniappan et al. 2010a) and thereby causing apoptosis in human HCC cell lines (Ganapathy-Kanniappan et al. 2010b; Yu et al. 2011). Hypoxia also can trigger accumulation of unfolded proteins in the ER and lead to ER stress (Xu et al. 2005). ER stress induces a stress response characterized by the up-regulation of ER chaperones and a cascade of transcriptional regulation allowing the cells to adapt and focus resources on damage repair. The unfolded protein response (UPR) is an important ER stress response which saves the cell by removing unfolded or misfolded proteins (Szegezdi et al. 2006). However, excessive and prolonged ER stress elicits apoptotic cell death. Many ER stress–response chaperones have protein disulfide isomerase (PDI) activity or PDI-like domains, and blocking this activity may be a way to augment ER stress and enhance apoptosis (Puig et al. 1994).

Based on this knowledge, we postulated that PDI might be one of the possible mechanisms of adaptation to ER stress, which could be induced by HK II inhibitor in hypoxic HCC cells. The aim of this study was to investigate if PDI is induced by hypoxia in HCC cells, and to evaluate the anti-tumor efficacy of a PDI inhibitor in an in vivo model of HCC. Moreover, we also investigated whether simultaneous treatment with 3-BP and a PDI inhibitor might synergistically enhance their anti-tumor efficacies against HCCs.

Materials and methods

Cell culture

Huh-7 and SNU-761 cell lines were used in this study. Cells were grown in DMEM supplemented with 10% fetal bovine serum, streptomycin (100 mg/L), and penicillin (100,000 U/L). Cells were proliferated with 3% fetal bovine serum, and in other experiments, cells were serum starved overnight to avoid serum-induced signals. Depending on the experiment, cells were incubated either under standard culture conditions (20% O_2 and 5% CO2, at 37 °C) or hypoxic conditions (1% O_2, 5% CO_2, and 94% N_2; at 37 °C).

Chemicals and reagents

3-BP and the PDI inhibitor, bacitracin, were obtained from Sigma-Aldrich, Inc. (St. Louis, MO, USA). SP600125 (a c-Jun NH2-terminal kinase (JNK) inhibitor) was obtained from Plymouth Meeting (Biomol Research Laboratories, PA, USA).

Quantitation of apoptosis

The degree of apoptosis was determined with nuclear binding dye 4′, 6-diamidino-2-phenylindole dihydrochloride (DAPI) by quantifying the apoptotic cells with fluorescence microscopy (Zeiss, Germany). Briefly, DAPI was added to the treated cells for 30 min, after which they were examined by fluorescence microscopy. Apoptotic cells were identified by chromatin condensation and nuclear fragmentation. The percentage of apoptotic cells was calculated as the ratio of

apoptotic cells to total cells counted × 100. A minimum of 400 cells was counted for each treatment.

Immunoblot analysis

Cells were lysed for 20 min on ice with lysis buffer (50 mM Tris–HCl, pH 7.4; 1% Nonidet P-40; 0.25% sodium deoxycholate; 150 mM NaCl; 1 mM EDTA; 1 mM phenylmethylsulfonylfloride; 1 μg/mL of each of aprotinin, leupeptin, and pepstatin; 1 mM Na_3VO_4; and 1 mM NaF) and then centrifuged at 14,000 g for 10 min at 4 °C. Samples were resolved by sodium dodecyl sulfate polyacrylamide gel electrophoresis, transferred to nitrocellulose membranes, blotted with the appropriate primary antibodies, and incubated with peroxidase-conjugated secondary antibodies (Biosource International, Camarillo, CA, USA). Bound antibodies were visualized with a chemiluminescent substrate (ECL; Amersham, Arlington Heights, IL, USA) and exposed to Kodak X-OMAT film. The primary antibodies used were as follows: mouse anti-phospho-eukaryotic initiation factor 2α (eIF2α) obtained from Santa Cruz Biotechnology, Inc. (Santa Cruz, CA, USA); mouse anti-PDI obtained from Affinity Bioreagents (Golden, CO, USA); rabbit anti-caspase 9, rabbit anti-caspase 7 and mouse anti-phospho-JNK obtained from Cell Signaling Technology Inc. (Denver, MA, USA); and rabbit anti-HIF-1α and goat anti-HK II obtained from Santa Cruz Biotechnology Inc. (Santa Cruz, CA, USA).

Animals

Animal experiments were done with 5-week old male C3H/He mice (Charles River Laboratories, Wilmington, MA, USA). Mice were housed under specific pathogen-free conditions and treated in accordance with the guidelines issued by the Institutional Animal Care and Use Committee of Seoul National University Hospital.

Mouse HCC model

We used a previously described established s.c. HCC mouse model (Yamashita et al. 2001). Briefly, 2.5×10^6 viable MH134 cells suspended in 0.1 mL of RPMI-1640 were injected subcutaneously to produce a bleb in the left flanks of the C3H/He mice. When the tumor volumes reached 0.5 ~ 1.0 cm^3, bacitracin was given i.m. for 12 consecutive days. Thirteen days after injecting bacitracin (0, 10 mg/kg, 50 mg/kg, or 100 mg/kg), the mice were sacrificed by exsanguination through cardiac puncture under general anesthesia (isoflurane inhalation). Tumor masses and liver tissues were then harvested, fixed in 10% formaldehyde, and cryopreserved. Next, animal experiments were done to examine the synergistic anti-tumor efficacy of 3-BP in combination with bacitracin. When the tumor volumes reached 0.5 ~ 1.0 cm^3, 3-BP (1 mg/kg) was administered i.p. with/without bacitracin (10 mg/kg), which was administered by i.m. daily for 9 consecutive days. Ten days after administering 3-BP with/without bacitracin, mice were sacrificed by exsanguination through cardiac puncture under general anesthesia induced by isoflurane inhalation. The tumor masses and liver tissues were harvested, fixed in 10% formaldehyde, and cryopreserved.

Tumor growth kinetics

An exponential model was selected to describe the tumor growth kinetics. The equation used after 3-BP and/or bacitracin administration was as follows: $V = V0 \times \exp(k \times T)$ where V0 and V are the tumor volumes at baseline and T days later, respectively, and k is the growth rate constant related to the tumor doubling time (Kim et al. 2009). Data were analyzed with a nonlinear mixed effect modeling (NONMEM) software program (version V, level 1.1, Double Precision), using the first-order conditional estimation method and the PRED routine (Beal 1984). Inter-individual variabilities for V0 and k were modeled using exponential random effect models (Kim et al. 2009). For example, the tumor volume at baseline was modeled as $V0i = V0 \times \exp(\eta i)$, where V0i is the tumor volume at baseline for individual i; V0 is the typical value for the tumor volume at baseline for the population, and ηi is a normally distributed random variable with the mean zero and the variance ω^2_{V0}. In addition, the residual variability was modeled using a combined additive and proportional error model. The combined error model is described as follows: $Yij = \hat{Y}ij \times (1 + \varepsilon_{ija}) + \varepsilon_{ijp}$ where Yij is the jth observed tumor volume in individual i; $\hat{Y}\ ij$ is the jth predicted tumor volume in individual i, and ε_{ija} and ε_{ijp} are normally distributed random variables for individual i and measurement j, with the mean zero and variances σ^2_a and σ^2_p, respectively.

Quantitative evaluation of the necrotic area

Hematoxylin and eosin (H&E) stain was applied to assess the morphological features of the necrotic tumor regions. ScanScope CS (Aperio Technologies, Inc., Vista, CA, USA) was used to scan the entire tissue sections at ×40 magnification. The histological images of the tissue sections were saved as digital images (in Joint Photographic Experts Group format) in a computer for the measurement of the percentage of necrosis. Aperio ImageScope v11.0.2.725 (Aperio Technologies, Inc., Vista, CA, USA) was used to draw boundaries around the entire tumor region and the region-defining interface between necrotic and viable tissues by hand and to measure the necrotic area of each tumor tissue section. The pink amorphous areas with glassy homogeneous

appearance on the H&E staining were considered to represent necrotic tissues, and the purple pixel area were considered to represent viable tissues (Zhou et al. 2010). The percentage of necrotic tissue from the H&E-stained sections was calculated by dividing the area of the largest cross-section by the area of necrosis (Zhou et al. 2010).

Apoptosis

Apoptosis in tumor tissues was investigated by TUNEL staining with ApoTag Peroxidase In Situ Apoptosis Detection Kits (Chemicon International, Temecula, CA, USA) after fixing fresh tissue in 4% paraformaldehyde. Positive TUNEL cells were counted in six different high-power fields at ×400 and averaged. Cell numbers were expressed as the percentages of the total cells and these were referred to as the apoptotic indexes.

Staining of hexokinase II

Immunohistochemical staining for goat anti-HK II (Santa Cruz Biotechnology Inc., Santa Cruz, CA, USA) on paraffin-embedded sections was done with Vectastain Elite ABC Kits (Vector Laboratories). Aperio ImageScope v11.0.2.725 (Aperio Technologies, Inc., Vista, CA, USA) was used to draw boundaries around the 6 different HK II expressed tumor regions by hand and to evaluate the extent and intensity of the HK II expression for each tumor tissue section using automated quantitative analysis.

Microvessel density and PDI expression

Immunohistochemical staining for anti-CD 31 (Vector Laboratories, Burlingame, CA, USA) and anti-PDI (Affinity Bioreagents, Golden, CO, USA) on paraffin-embedded sections was done with Vectastain Elite ABC Kits (Vector Laboratories). CD 31-positive microvessels within the most vascular areas of the tumor tissues were counted in 6 different high-power fields at ×400 and averaged (Kim et al. 2009). The intra-tumoral mean microvessel density (MVD) was expressed as numbers of microvessels/mm^2.

Association of PDI with $\alpha_v\beta_3$ integrin

Double staining for anti-PDI (Affinity Bioreagents, Golden, CO, USA) and anti-$\alpha_v\beta_3$ integrin (Chemicon, Temecula, CA, USA) on paraffin-embedded sections was done with EnVision DuoFLEX Doublestatin System (Dako). The visualization was based on peroxidase (HRP) using DAB+ as a chromogen and on alkaline phosphatase (AP) using Permanent Red as a chromogen.

Immunoprecipitation analysis

Tumor tissue lysates were incubated with mouse anti-sera against PDI overnight at 4 °C. Immune complexes were immunoprecipitated with 20 μL of protein A/G PLUS agarose beads (Santa Cruz Biotechnology Inc.) for 2 h at 4 °C and then washed five times with lysis buffer. Polypeptides were then resolved by boiling with 35 μL of Laemmli sample buffer for 5 min, and the obtained immunoprecipitates were immunoblotted with anti-$\alpha_v\beta_3$ integrin (Chemicon, Temecula, CA, USA).

Statistical analysis

All cell-based experimental data were acquired from at least three independent experiments from a minimum of three separate isolations and were expressed as the means ± standard deviations (SD). Statistical evaluations of numerical variables in each group were done with the Mann-Whitney *U* test and the Kruskal-Wallis test. All statistical analyses were done with SPSS version 17.0 (SPSS, Inc., Chicago, IL, USA). Statistical significance was accepted for P values of <0.05.

Results

Hypoxia-induced ER stress and PDI expression in HCC cells

We first investigated whether ER stress and PDI expression were hypoxia-inducible in HCC cells. Hypoxia increased the phosphorylation of eIF2α (Fig. 1a) and the expression of

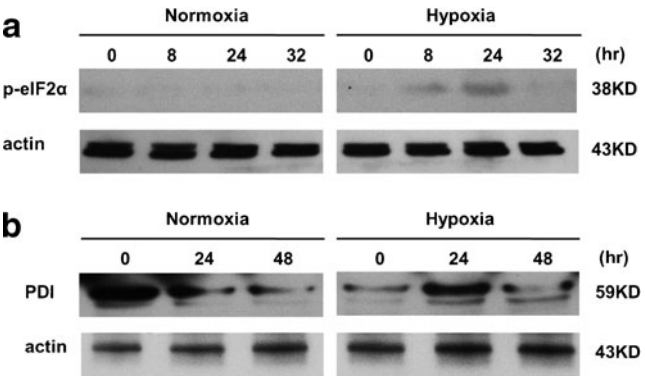

Fig. 1 Hypoxia-induced ER stress and PDI expression in a human HCC cell line. **a** Hypoxia induced ER stress in HCC cells. SNU-761 cells were cultured under normoxic or hypoxic conditions for the indicated times. Equivalent amounts of proteins were immunoblotted with anti-phospho-eIF2α and anti-actin antibodies. **b** Hypoxia induced PDI expression in HCC cells. PDI expression was promptly induced under hypoxic conditions. SNU-761 cells were cultured under normoxic or hypoxic conditions for the indicated times. Equivalent amounts of proteins were immunoblotted using anti-PDI and anti-actin antibodies

PDI (Fig. 1b) in Huh-7 cells. This finding implicates that HCC cells do express PDI and its expression is hypoxia-inducible in HCC cells.

Enhanced HK II inhibitor-induced apoptosis by PDI inhibition in HCC cells

Since hypoxia induces HK II (Gwak et al. 2005) and expression of PDI (Graven et al. 2002), we postulated that simultaneous blockage of these two enzymes would enhance HK II inhibitor (3-BP)-induced apoptosis in HCC cells under hypoxic conditions. When PDI-inhibited HCC cells (bacitracin-treated) were treated with 3-BP under hypoxic conditions, apoptosis was significantly enhanced as compared to the cells treated with just 3-BP (Fig. 2a).

Mechanism of enhanced apoptosis by PDI inhibition

To explore the possible mechanism of 3-BP-induced apoptosis enhancement by PDI inhibition, we then explored which apoptotic signals were more activated in 3-BP/PDI

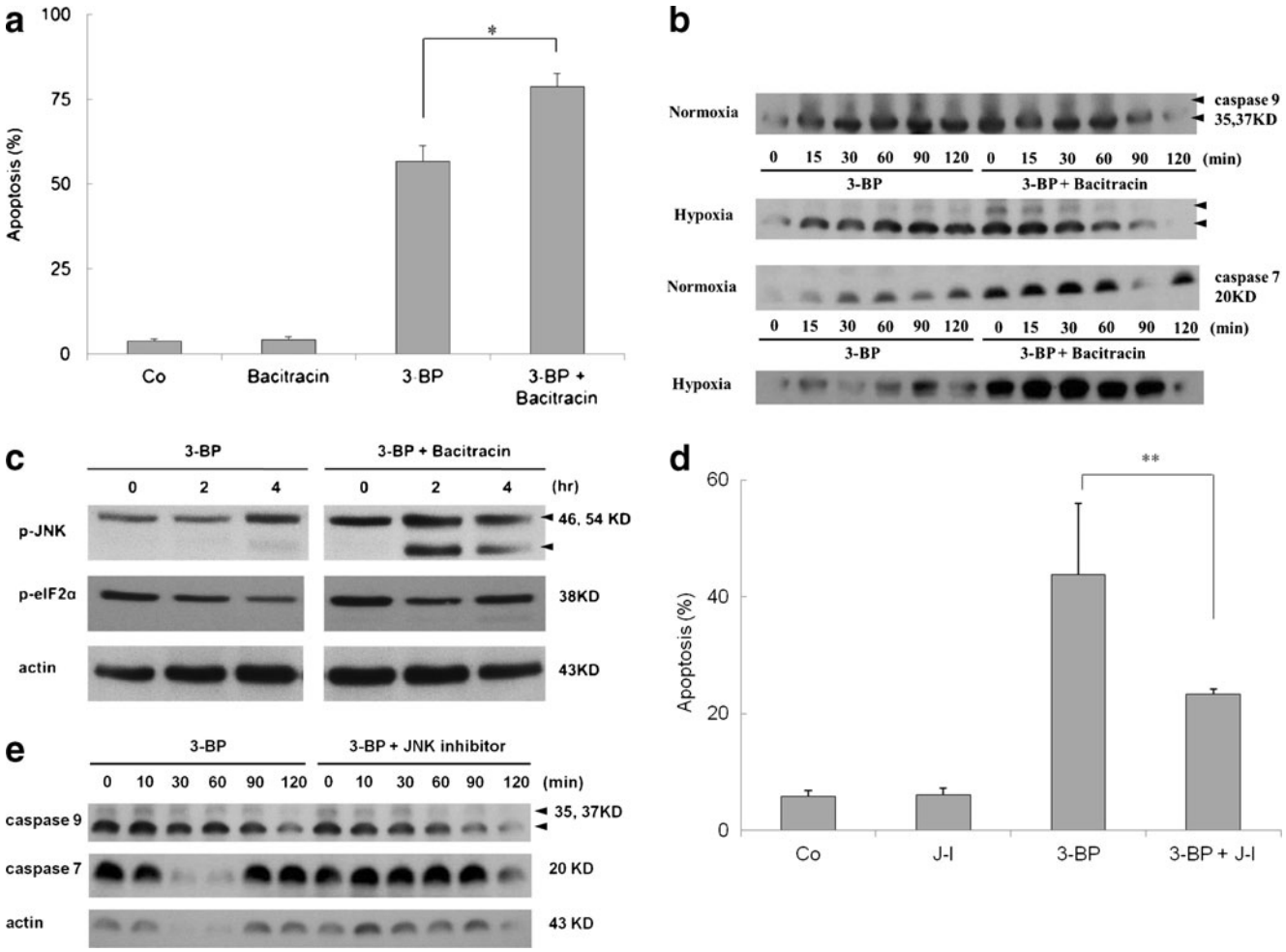

Fig. 2 Enhancement of HK II inhibitor-induced apoptotic cell death by PDI inhibition. **a** Huh-7 cells were serum starved for 24 h and then treated with 3-BP (100 μM) in the presence or absence of bacitracin (0 and 5 mM) treatment. Apoptotic cells were counted by DAPI staining and fluorescent microscopy. **b** Activation of caspase 9 and 7 was more prominent in 3-BP + bacitracin-treated cells compared to the cells treated with just 3-BP and **c** PDI inhibition induced ER stress-dependent JNK activation. Huh-7 cells were serum starved and cultured under normoxic or hypoxic conditions and then treated with 3-BP (100 μM) in the presence or absence of bacitracin (0 and 5 mM) for the indicated times. Cells were lysed and immunoblot analysis was done with anti-phospho-JNK, anti-phospho-eIF2α, and anti-actin antibodies. **d** JNK activation participated in 3-BP-induced apoptosis. Huh-7 cells were serum starved for 24 h under hypoxic culture conditions and then treated with 3-BP (0 and 100 μM) and/or JNK inhibitor (0 and 10 μM) for 6 h. Apoptotic cells were counted by DAPI staining and fluorescent microscopy. **e** Activation of caspase 9 and 7 was suppressed in 3-BP + JNK inhibitor-treated cells compared to the cells treated with just 3-BP. Huh-7 cells were serum starved for 24 h and then treated with 3-BP (100 μM) in the presence or absence of JNK inhibitor (0 and 5 mM) treatment. Cells were lysed and immunoblot analysis was done with anti-caspase 9, anti-caspase 7, and anti-actin antibodies. Data were expressed as the mean ± SD. *, P=0.001. **, P=0.004. J-I represents JNK inhibitor

inhibitor-treated cells compared to the cells treated with just 3-BP. When the cells were treated with 3-BP and PDI inhibitor, the activation of caspase 9 and 7 was more prominent than in the cells treated with just 3-BP (Fig. 2b), indicating that activation of mitochondrial apoptotic signaling is augmented by PDI inhibition. We then explored kinase signals that regulated apoptosis and found that pro-apoptotic JNK was more promptly and potently activated in cells treated with 3-BP and PDI inhibitor than in the cells treated with just 3-BP (Fig. 2c). Since JNK activation may depend on ER stress, we then evaluated whether ER stress was activated in 3-BP and PDI inhibitor-treated cells. Indeed, as shown in Fig. 2c, eIF2α phosphorylation, which reflects ER stress activation, was prominent in these cells. Finally, we examined whether JNK activation participated in 3-BP-induced apoptosis enhancement by PDI inhibition, and found that JNK inhibition did attenuate this enhancement (Fig. 2d). When the cells were treated with both 3-BP and the JNK inhibitor, the activation of caspase 9 and 7 was less prominent than in the cells treated with just 3-BP (Fig. 2e). Therefore, these findings collectively suggest that PDI inhibition may induce ER stress-dependent JNK activation in 3-BP-treated HCC cells and thus, enhance apoptotic cell death in these cells.

Anti-tumor efficacy of PDI inhibitor in an in vivo model of HCC

To evaluate the anti-tumor efficacy of PDI inhibitor in an in vivo model of HCC, we established an animal model of HCC in C3H mice by i.d. implanting MH134 cells. MH134 cells effectively produced tumors in the control mice within 14 days of i.d. injection. Tumor-bearing mice were then treated with bacitracin (0, 10, 50, and 100 mg/kg, i.m. daily for 12 days). The anti-tumor efficacy of bacitracin was first evaluated by measuring the tumor volumes. The tumor volumes in the bacitracin-treated mice showed a tendency to decrease compared to the control mice in a dose-dependent manner (the mean tumor volume, 6.66 versus 5.70 versus 3.73 versus 2.74 cm^3 in the bacitracin-treated mice at 0, 10, 50, and 100 mg/kg/day, respectively; $P=0.064$; Fig. 3a). Pathological evaluations revealed that regions of central necrosis had developed in most tumors (Fig. 3b). The percentage of the necrotic area per total tumor area was significantly different between the control and the bacitracin-treated tumors (24.2 versus 42.3 versus 56.6 versus 46.6% in the bacitracin-treated mice at 0, 10, 50, and 100 mg/kg/day, respectively; $P<0.001$; Fig. 3b).

We next evaluated whether bacitracin induced apoptosis in mouse HCC tumors. To quantify apoptosis in tumors, we first used TUNEL staining. However, the percentages of TUNEL-stained cells were not different between the control group and the bacitracin–treated groups ($P=0.102$; Fig. 4a). Since bacitracin showed a marginal anti-tumor effect, we then explored the underlying mechanism in the anti-tumor efficacy of the PDI inhibitor using MVDs. The mean MVDs were significantly decreased in the bacitracin-treated groups compared to the control group ($P<0.001$; Fig. 4b). Immunohistochemical staining of anti-PDI showed that PDI was expressed on the surface of vascular endothelial cells as well as tumor cells. In addition, the percentage of PDI-stained vascular densities was significantly decreased in bacitracin-treated mice in a dose-dependent manner (Fig. 4c).

Intra-tumoral hypoxia-induced HK II expression

We then explored whether an intra-tumoral hypoxic environment induced HK II expression in the in vivo model. Indeed, immunohistochemical staining for anti-HK II revealed that HK II was strongly expressed in the viable tumor tissues near necrotic region even in the control group. The extent ratio of HK II was significantly different between the control and the bacitracin-treated tumors (1 versus 1.75 versus 2.12 versus 2.81 in the bacitracin-treated tumors at 0, 10, 50, and 100 mg/kg/day, respectively; $P<0.001$; Fig. 4d). The intensity ratio of HK II was also significantly different between the control and the bacitracin-treated tumors (1 versus 1.67 versus 2.02 versus 2.70 in the bacitracin-treated tumors at 0, 10, 50, and 100 mg/kg, respectively; $P<0.001$; Fig. 4d).

In vivo synergistic anti-tumor efficacy of the HK II and PDI inhibitors

We then evaluated whether 3-BP and bacitracin had a synergistic anti-tumor effect in an in vivo model of HCC. Indeed, the mean tumor volumes were significantly reduced in mice treated with 3-BP and bacitracin compared with the control, 3-BP-treated, or bacitracin-treated mice (Fig. 5a). The synergistic effect was examined with NONMEM assuming an exponential tumor growth kinetic curve. The growth rate constants were significantly longer for 3-BP + bacitracin-treated mice than for untreated controls, 3-BP-treated, or bacitracin-treated mice, demonstrating that 3-BP and bacitracin acted synergistically to inhibit tumor growth (Table 1).

We examined if regions of central necrosis were higher in mice treated with 3-BP + bacitracin compared with the control, 3-BP-treated, or bacitracin-treated mice with H&E staining (Fig. 5b). The percentage of necrotic areas per total tumor area was significantly different between the control, 3-BP-treated, bacitracin-treated, and 3-BP + bacitracin-treated tumors (18.0 versus 27.6 versus 29.6 versus 53.6%; $P=0.038$; Fig. 5b). When we explored the expression level

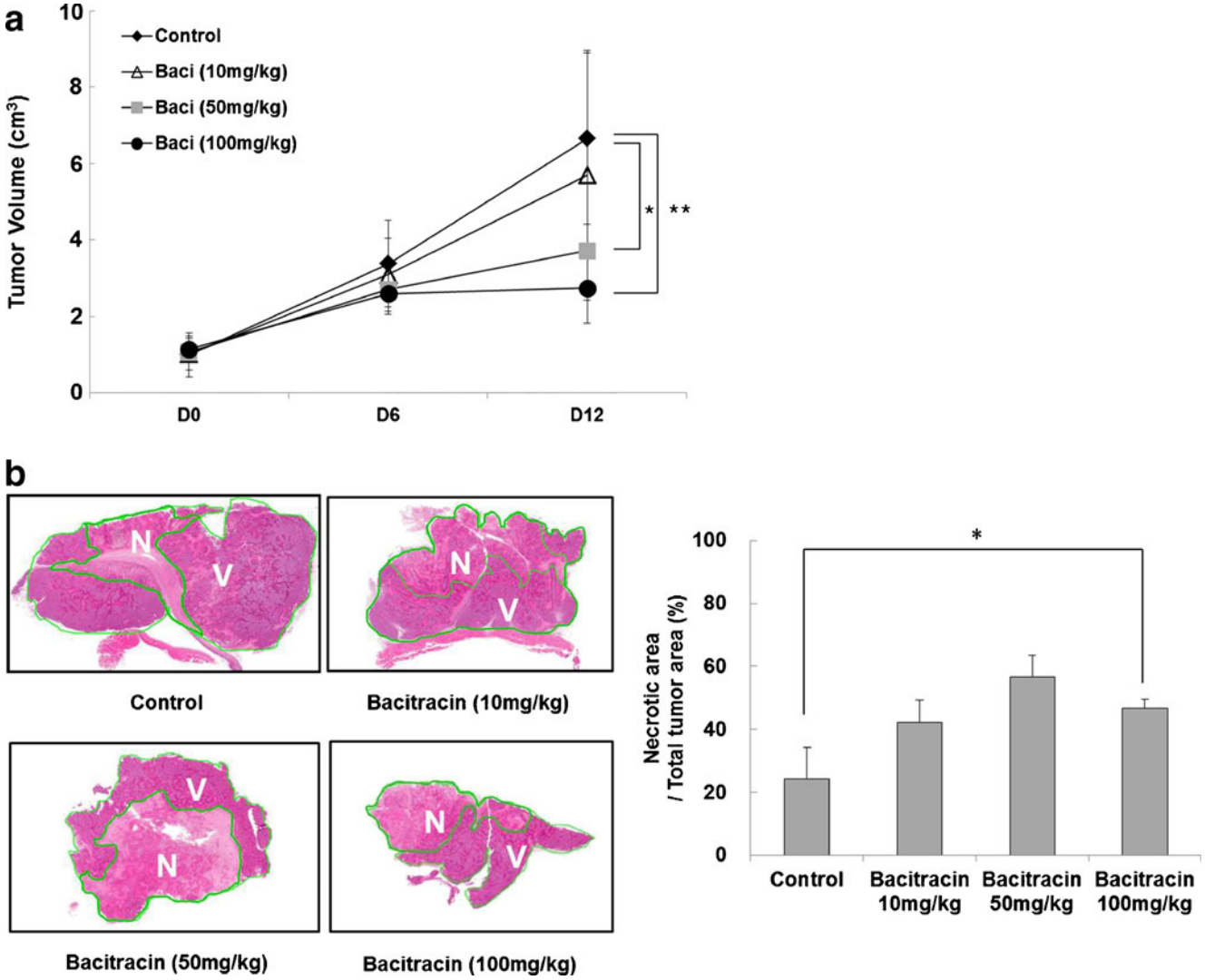

Fig. 3 In vivo anti-tumor efficacy of the PDI inhibitor, bacitracin. In mice bearing MH134 tumors, bacitracin was given (0, 10, 50, and 100 mg/kg daily i.m. for 12 d). **a** Tumor volumes were calculated by measuring the tumor lengths (L) and widths (W) of the sagittal sections and calculated as follows: $0.5 \times L$ (cm) $\times W^2$ (cm^2). Four mice were randomly allocated into each of these bacitracin dosage groups. Points, mean tumor volumes; *bars*, SD. *, $P=0.083$ versus control. **, $P=0.064$ versus control. **b** H&E staining images showing that central necrosis (area designated N) developed within the tumor tissue (bacitracin 0, 10, 50, and 100 mg/kg/day group, respectively). Original magnification, ×40. Central necrosis was estimated by dividing the necrotic area with the total tumor area. Columns, the means of four independent cases; *bars*, SD. *, $P<0.001$. N represents necrotic tissue. V represents viable tissue

of HK II in the in vivo model, HK II was significantly over-expressed in the bacitracin-treated group compared to the control group and this over-expression was significantly suppressed by the combinatorial treatment of 3-BP + bacitracin (Fig. 5c).

We next evaluated whether apoptotic levels were higher in 3-BP + bacitracin-treated mice compared with the control, 3-BP-treated, or bacitracin-treated mice using TUNEL staining. In addition, since the PDI activity might be related to angiogenesis, we also evaluated the anti-angiogenic effects of these treatments by comparing the MVDs. As shown in Fig. 6a and b, the percentages of TUNEL positive cells were significantly increased and the mean MVDs were significantly decreased in mice treated with 3-BP + bacitracin compared to the other three treatments, respectively ($P<0.05$).

Finally, since PDI was reported to be found on the surface of endothelial cells (Jordan and Gibbins 2006), we explored if this anti-angiogenic effect of bacitracin was related to the association of PDI with $\alpha_v\beta_3$ integrin which was alleged to be involved in the maturation of blood vessels (Drake et al. 1995). As shown in Fig. 6c, $\alpha_v\beta_3$ stained vessels were significantly decreased in the bacitracin-treated mice compared to the control or 3-BP treated group. To investigate

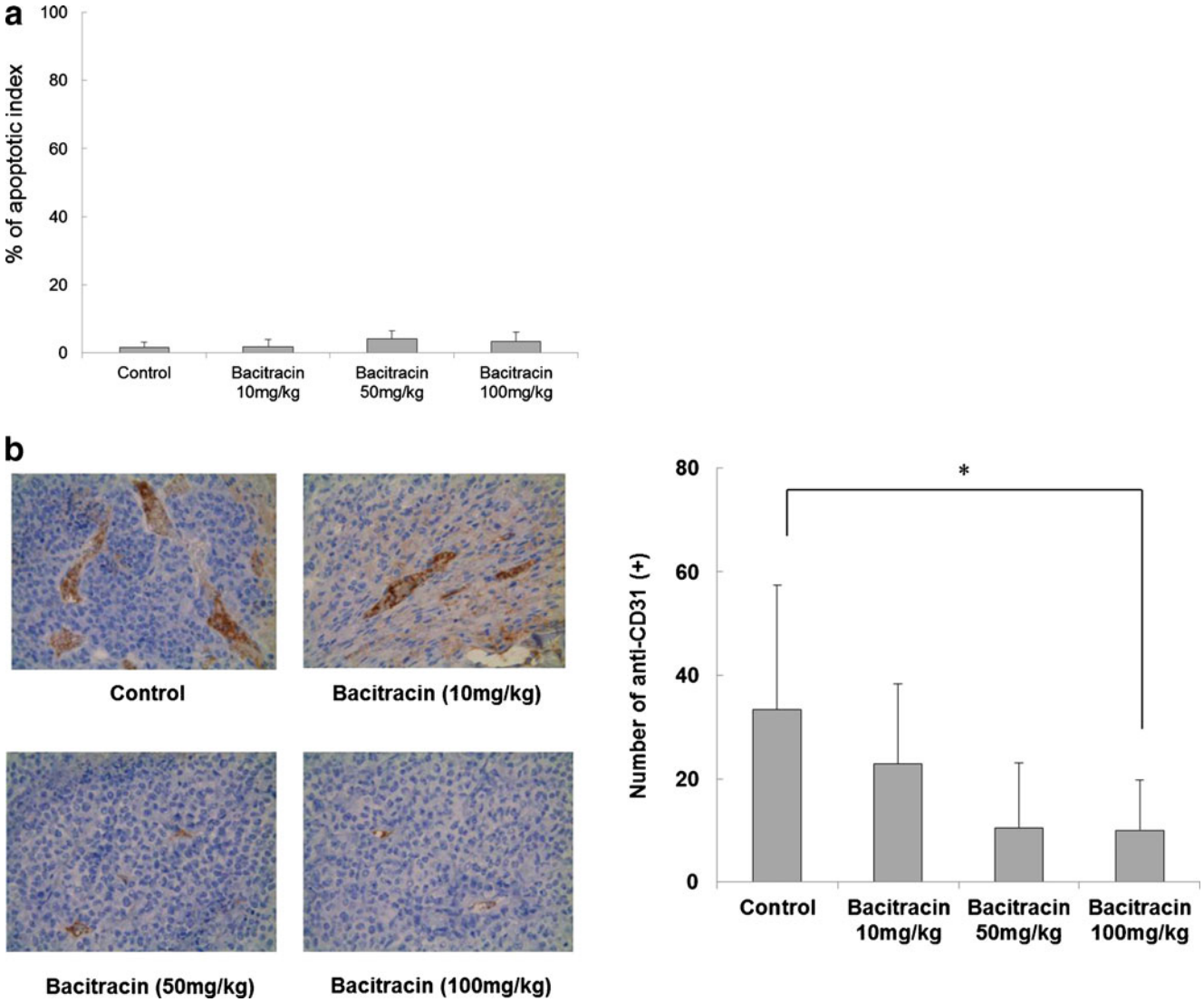

Fig. 4 In vivo demonstration of the anti-tumor efficacy of the PDI inhibitor, bacitracin. **a** Apoptotic indexes compared by TUNEL staining were not significantly different between the control group and bacitracin–treated group. **b** Mean MVDs were significantly decreased in mice treated with bacitracin. Intra-tumoral MVDs in the mice treated with bacitracin (dosage groups) were compared by immunohistochemical staining. Mean MVDs were determined by counting CD31 + vessels in 6 different high-power fields (×400) and averaged. Columns, mean values of each group; *bars*, SD. *, $P<0.001$. **c** PDI-stained vascular densities were significantly decreased in mice treated with bacitracin. Intra-tumoral PDI-stained vascular densities in the mice treated with bacitracin (dosage groups) were compared by immunohistochemical staining. Columns, mean values of each group; *bars*, SD. *, $P<0.001$. Mean PDI-stained vascular densities were determined by counting PDI + vessels in 6 different high-power fields (×400) and averaged. **d** HK II expression in HCC tumor tissue. Immunohistochemical staining for anti-HK II revealed that the extent and intensity ratio of HK II were significantly different between the control and bacitracin-treated tumors. Columns, mean values of each group; *bars*, SD. *, $P<0.001$. Original magnification, ×100

the possible mechanism of this finding, PDI was immunoprecipitated from the tumor tissue lysates, and the PDI levels and PDI to $\alpha_v\beta_3$ integrin binding affinity were evaluated by immunoblotting these precipitates with antibodies for PDI and $\alpha_v\beta_3$ integrin. As shown in Fig. 6d, bacitracin decreased both PDI expression and the association between PDI and $\alpha_v\beta_3$ integrin. These findings collectively suggest that 3-BP and bacitracin act synergistically in vivo, and that their anti-tumor effects involve enhancing apoptosis and reducing angiogenesis.

Discussion

The principal findings of this study are related to the synergistic effect of PDI inhibition on HK-II inhibitor-induced anti-tumor efficacy in HCC cells. In particular, this study demonstrated that hypoxia stimulates the expression of PDI in HCC cells and revealed the anti-angiogenic effect of PDI inhibition in an in vivo model of HCC. In addition, the inhibition of PDI enhanced 3-BP-induced apoptotic cell death mediated by ER stress-dependent JNK activation.

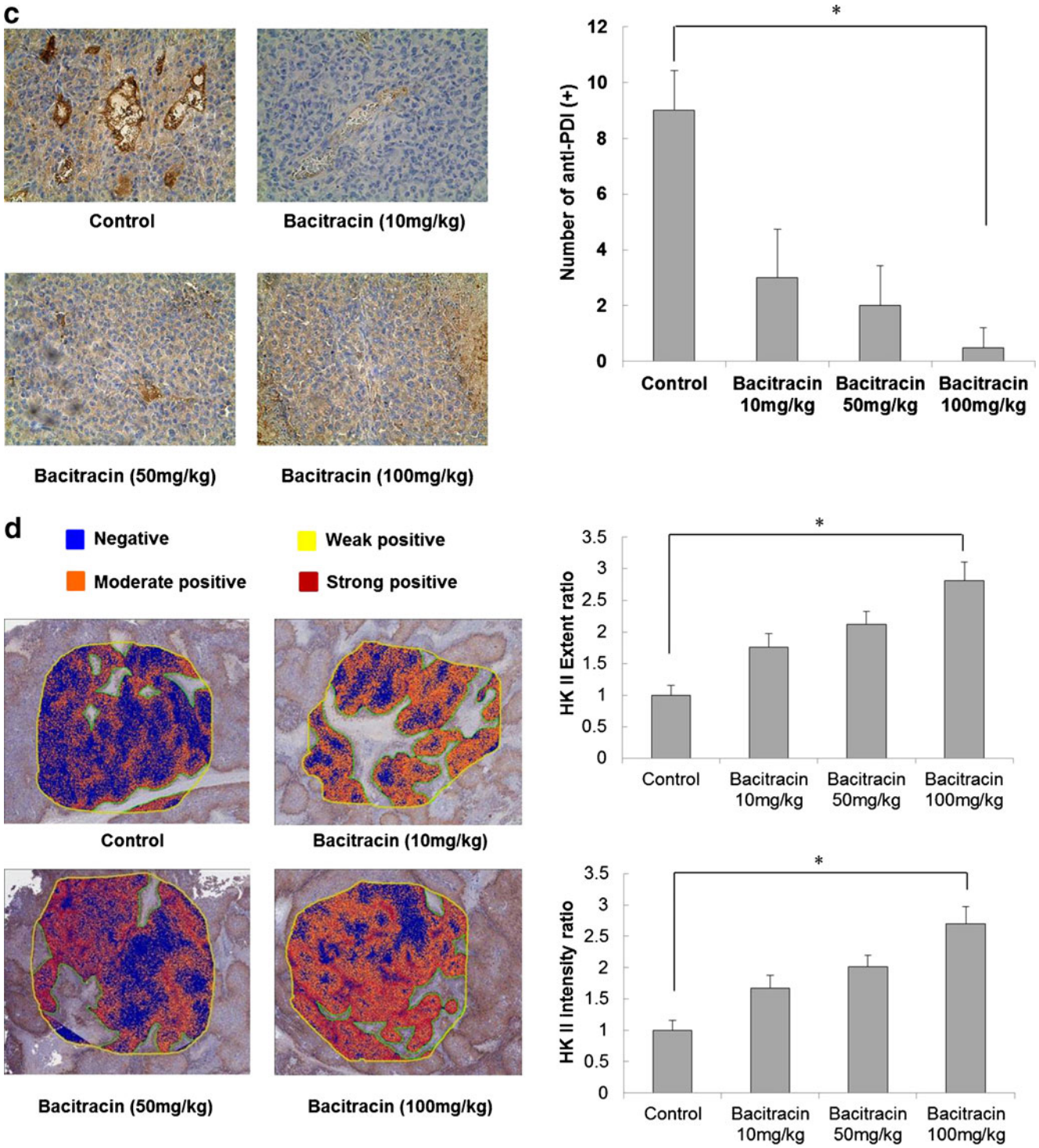

Fig. 4 (continued)

Moreover, the synergistic anti-tumor efficacy of HK II and PDI inhibitors was confirmed in mice bearing HCCs. Each of these findings will be discussed below.

Previous studies have shown that the expression of PDI family proteins correlates with cancer invasion, metastasis, and drug resistance in various tumor types including melanoma and glioma (Tager et al. 1997; Goplen et al. 2006). Although PDI expression was reported to be increased in the stressful microenvironment of human HCC cell lines and in the serum of HCC patients (Feng et al. 2007; Chignard et al. 2006), its functional implications in HCC were not fully elucidated. We used bacitracin as a PDI

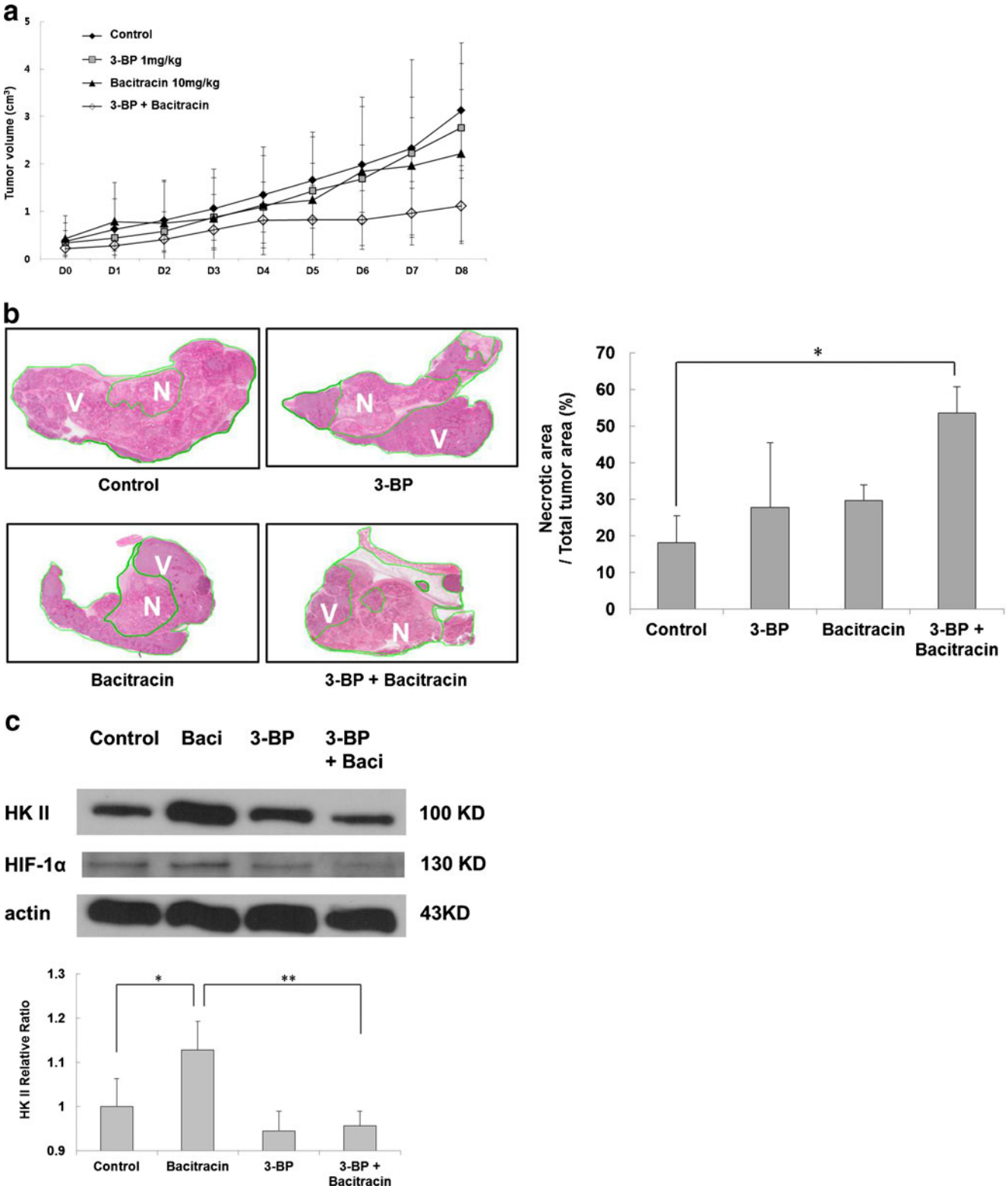

inhibitor to examine the functional profiles of PDI in HCC cells. The peptide antibiotic, bacitracin, was reported to be an inhibitor of PDI in 1981 (Roth 1981) and since then, has been widely used to demonstrate the role of PDI in cellular processes. Bacitracin acts as an antibiotic by forming a complex between divalent cations and the bacterial C55-isoprenyl lipid carrier, ultimately resulting in the inhibition of cell wall biosynthesis (Ming and Epperson 2002). Although the

◀ **Fig. 5** In vivo synergistic anti-tumor efficacy of the HK II and PDI inhibitors. **a** An in vivo model of HCC was established in C3H mice by implanting MH134 cells subcutaneously. 3-BP (0, 1 mg/kg, i.p.) and/or bacitracin (0, 10 mg/kg, i.m.) were administered to the mice for 8 days after tumor volumes had reached 0.5~1.0 cm^3. Tumor volumes were calculated as follows: 0.5×L (cm)×W^2 (cm^2), where L and W represent maximum length and width, respectively. Six mice were randomly allocated to each group. Points, mean tumor volumes; bars, SD. **b** H&E staining images showing that central necrosis (area designated N) developed within the tumor tissue (control, 3-BP, bacitracin, and 3-BP + bacitracin groups, respectively). Original magnification, ×40. Central necrosis was estimated by dividing the necrotic area with the total tumor area. Columns, the means of 6 independent cases; *bars*, SD. *, $P<0.001$. N represents necrotic tissue. V represents viable tissue. **c** Tumor tissues were harvested, and equivalent amounts of proteins were immunoblotted with anti-HK II, anti-HIF-1α and anti-actin antibody. Columns, the means of four independent cases; *bars*, SD. *, $P<0.001$. **, $P<0.001$

mechanism of the inhibitory action of bacitracin on PDI is still unclear, a recent study has shown that a direct interaction of bacitracin with PDI involves the formation of a disulfide bond between an open thiol form of the bacitracin thiazoline ring and the cysteines in the substrate-binding domain of PDI (Dickerhof et al. 2011).

In this study, it was observed that PDI was expressed in a human HCC cell line under hypoxic culture conditions. This finding implicates that PDI may participate in UPR to compensate for the ER stress under innate intra-tumoral hypoxic conditions or hypoxic insult, such as, TACE. Given the IC_{50} value (70 μM) for the inhibition of PDI activity by commercial bacitracin, we used a sufficient concentration of bacitracin (5 mM) to suppress cellular growth in vitro (Dickerhof et al. 2011). In addition, considering that the recommended dose of bacitracin for the treatment of staphylococcal pneumonia was 10–40 mg/kg/day in infants (Briggs 1957), we evaluated the anti-tumor efficacy of bacitracin at different dose levels (0, 10, 50, 100 mg/kg/day) in vivo. However, when examined in this study, bacitracin alone did not induce significant cellular apoptosis in vitro or in vivo. This might be related to the other arms of UPR; tumor cells can regulate their ER stress by translational attenuation with PKR-related ER kinase (PERK), transcriptional induction with inositol requiring enzyme-1 (IRE1), X-box binding protein-1 (XBP-1) (Ron and Walter 2007), activating transcription factor (ATF) 6 (Moenner et al. 2007), and ER-associated degradation as well as via posttranslational modifications with PDI (Mori 2000).

In this study, bacitracin had a trend to suppress tumor growths and the formation of intra-tumoral central necrosis. Although bacitracin did not induce statistically significant cellular apoptosis, the mean MVDs were significantly decreased in the bacitracin-treated groups compared to the control group in vivo. Since PDI was reported to be up-regulated in vascular endothelial cells in the viable peri-infarct and infarct regions of mouse hearts and involved in angiogenesis (Tian et al. 2009), we examined if PDI was expressed on the vascular endothelial cells of tumor tissues. Indeed, we found that PDI was expressed on vascular endothelial cells of tumor tissues and bacitracin suppressed PDI expression in a dose-dependent manner. These observations suggest that bacitracin treatment might have an anti-tumor efficacy by suppressing the PDI activity involved in angiogenesis (Tian et al. 2009). Although bacitracin has possible anti-angiogenic effects, bacitracin alone could not induce a significant anti-tumor effect in vivo. This finding

Table 1 Development of the tumor growth kinetics model by forward addition to the base model and backward elimination from the full model

Hypothesis	−2 * Log-likelihood	DF	Diff (−2 * log-likelihood)	Chi-square (α=0.05)	P-value	Conclusion
Base model						
K value of each group was identical. (K1=K2=K3=K4)	441.2	2				
Full model						
Was k different according to treatment group?	460.1	5	18.9	7.81 (df=3)	0.0003	YES
backward elimination from the Full model						
Was k different between control group & 3-BP-treated group?	460.4	4	−0.3	3.84 (df=1)	0.5839	NO
Was k different between control group & bacitracin-treated group?	462	4	−1.9	3.84 (df=1)	0.1681	NO
Was k different between control group & combination-treated group?	456.8	4	3.3	3.84 (df=1)	0.0693	YES
Was k different between 3-BP-treated group & bacitracin-treated group?	460.8	4	−0.7	3.84 (df=1)	0.4028	NO
Was k different between 3-BP-treated group & combination-treated group?	454.2	4	5.9	3.84 (df=1)	0.0151	YES
Was k different between bacitracin-treated group & combination-treated group?	450	4	10.1	3.84 (df=1)	0.0015	YES
Final model	460.1					

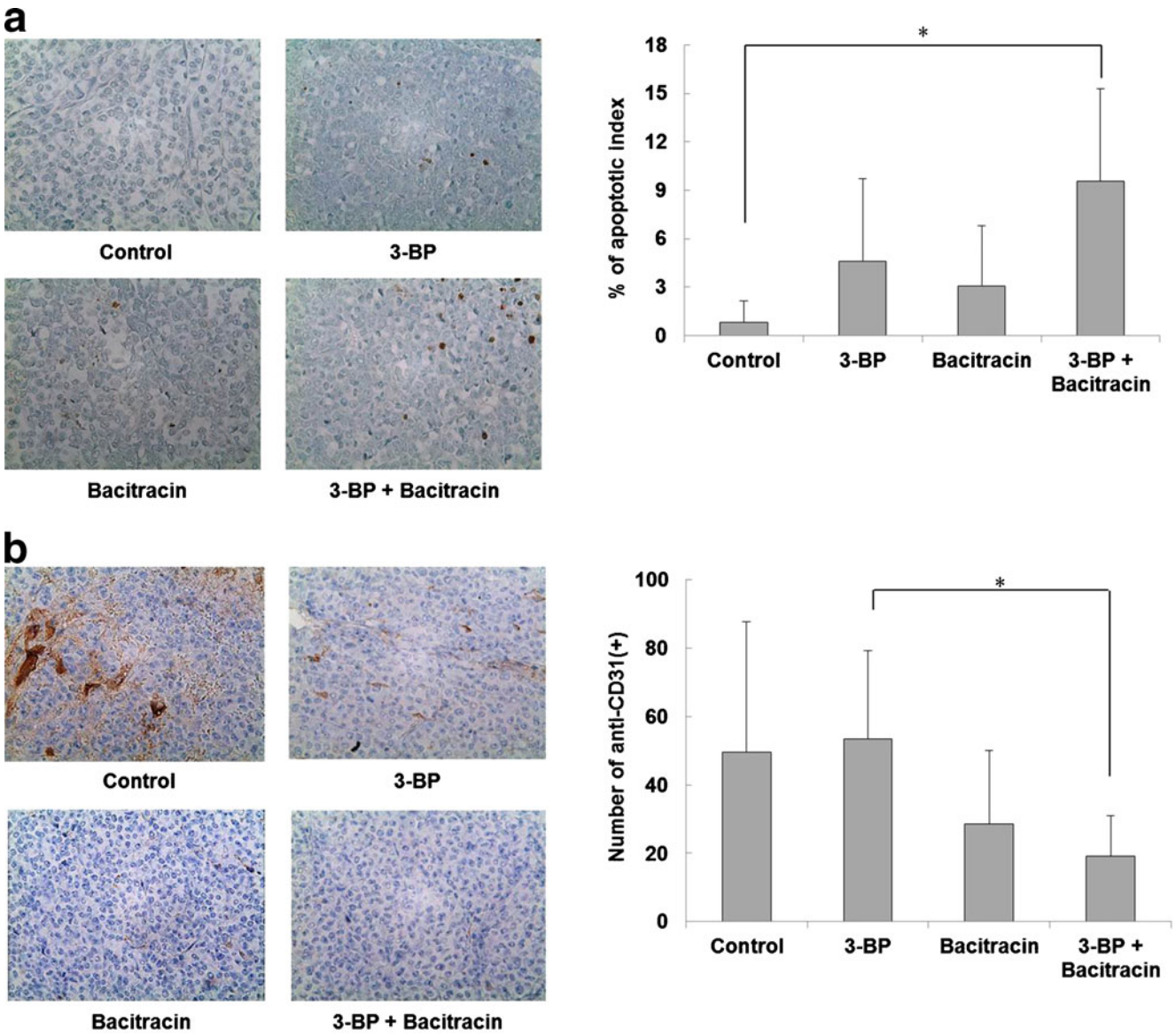

Fig. 6 The mechanism of the synergistic effect of the HK II and PDI inhibitors. **a** TUNEL-positive cell proportions were significantly increased in mice treated with 3-BP + bacitracin. Apoptosis in tumor tissues were assessed by TUNEL staining after fixing fresh tissues in 4% paraformaldehyde. Positive stained cells were counted in 6 different high-power fields (×400) and averaged. Cell numbers are expressed as percentages of the total cells, and are referred to as apoptotic indexes. Columns, mean values of each group; *bars*, SD. *, $P<$ 0.001. **b** The mean MVDs were significantly decreased in mice treated with 3-BP + bacitracin. Intra-tumoral MVDs in mice treated with 3-BP and/or bacitracin were compared by immunohistochemical staining. The mean MVDs were determined by counting CD31 + vessels in 6 different high-power fields (×400) and averaged. Columns, mean values of each group; *bars*, SD. *, $P=0.030$. **c** Double staining of PDI and $\alpha_v\beta_3$ integrin revealed that $\alpha_v\beta_3$ integrin-stained vascular densities were significantly decreased in mice treated with 3-BP + bacitracin. Intra-tumoral $\alpha_v\beta_3$-stained vascular densities in mice treated with 3-BP and/or bacitracin were compared by immunohistochemical staining. The mean $\alpha_v\beta_3$-stained vascular densities were determined by counting $\alpha_v\beta_3$ + vessels in 6 different high-power fields (×400) and averaged. Columns, mean values of each group; *bars*, SD. *, $P=0.030$. **d** Tumor tissues were lysed and PDI was immunoprecipitated. Immunoblotting was done for PDI and $\alpha_v\beta_3$ integrin. Columns, mean values of each group; *bars*, SD. *, $P=0.038$

can be explained because when angiogenesis is attenuated by bacitracin, hypoxic HCCs are likely to progress further by up-regulation of hypoxia-induced survival signals, such as HK II (Yoon and Lee 2008; Gwak et al. 2005). Indeed, immunohistochemical staining of tumor tissues confirmed that HK II expression was up-regulated in a dose-dependent manner in the bacitracin-treated group compared to the control group. These findings suggest the possibility that the anti-tumor effects of bacitracin can be increased in combination with HK II inhibitor (3-BP), since 3-BP uptake in HCC cells is maximized by high HK II expression levels (Kim et al. 2007).

Since hypoxia, which is a hallmark of solid tumors (Rapisarda and Melillo 2009), induces both HK II(Gwak

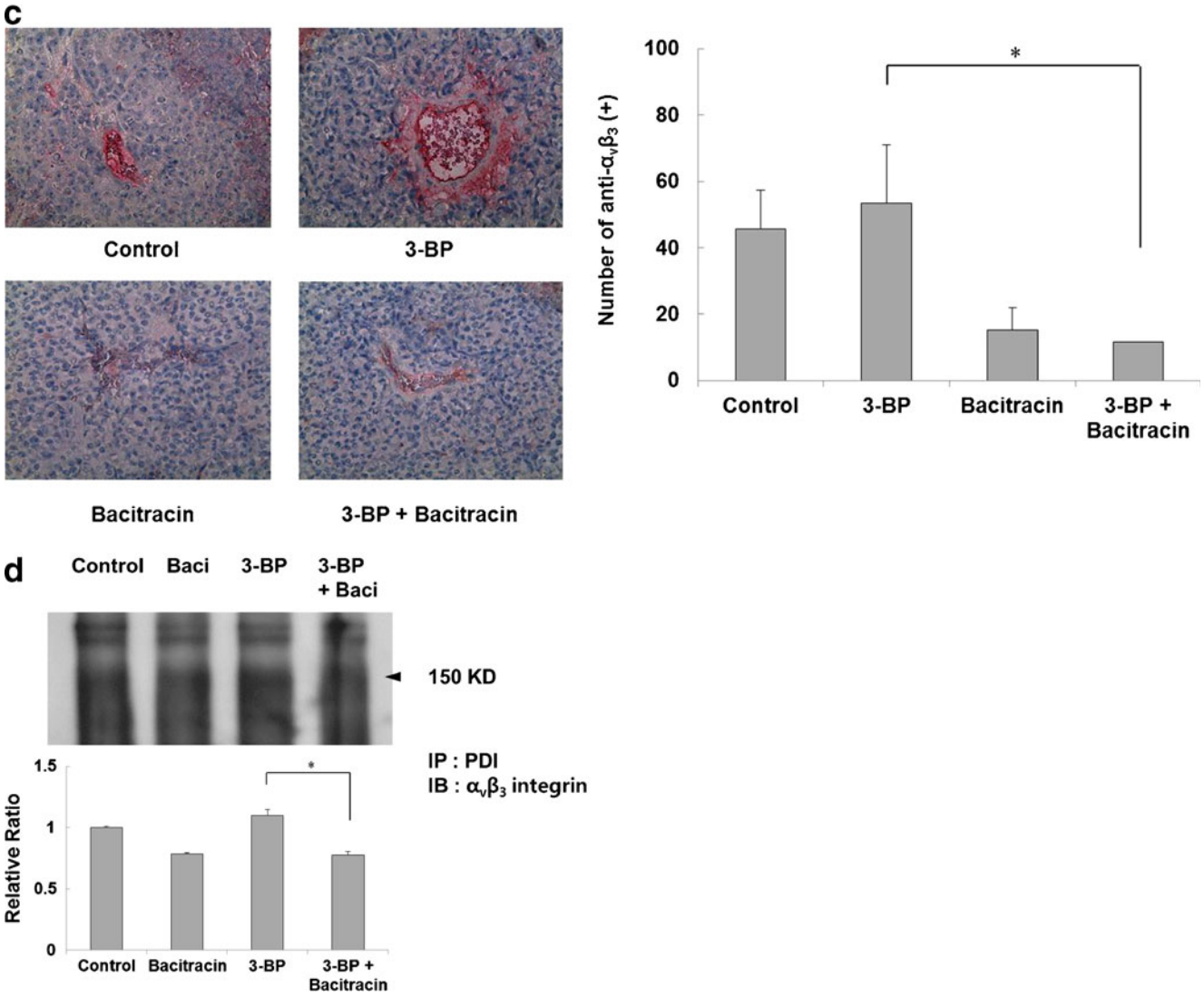

Fig. 6 (continued)

et al. 2005) and PDI (Chignard et al. 2006), we also postulated that simultaneous inhibition of these two enzymes could enhance HK II inhibitor-induced apoptosis in HCC cells. We confirmed that 3-BP-induced HCC cell apoptosis was significantly enhanced by PDI inhibition under hypoxic conditions. We then explored the possible mechanisms of the enhanced apoptosis by PDI inhibition and found that the activation of caspase 9 and 7 by 3-BP + bacitracin was more prominent than the activation induced by 3-BP alone, which suggests that the activation of mitochondrial apoptotic signaling is augmented by PDI inhibition. In a recent study, it has been reported that 3-BP may induce ER stress and thereby cause apoptosis in human HCC cell lines (Ganapathy-Kanniappan et al. 2010b; Yu et al. 2011). Since ER stress induction may activate JNK (Pastorekova et al. 2008; Szegezdi et al. 2006), we then evaluated whether ER stress was more activated in 3-BP and PDI inhibitor-treated cells than in the cells treated with just 3-BP and found that eIF2α phosphorylation was more prominent in the 3-BP and PDI inhibitor-treated cells. ER stress sensors initiate UPR resulting in transcriptional up-regulation of molecular chaperones including PDI (Mori 2000). This suggests that 3-BP-provoked ER stress may induce PDI expression as one of the UPRs to reduce ER stress. Thus, the simultaneous inhibition of PDI and HK II may disturb the compensating effect of ER stress, thereby leading to ER stress augmentation and subsequent JNK activation and enhancement of apoptosis through the mitochondrial activation of caspase 9 and caspase 7. Indeed, in the present study, we observed that JNK inhibition attenuated the enhanced apoptosis by HK II inhibitor. Moreover, bacitracin significantly enhanced 3-BP-induced HCC cell apoptosis shown by a greater number of

TUNEL-positive cells in the 3-BP + bacitracin-treated mice than in the 3-BP-treated mice. These findings indicate that PDI inhibition augments the apoptotic effect of 3-BP in HCC cells.

In the present study, the mean MVDs were significantly decreased in the 3-BP + bacitracin-treated mice compared to the 3-BP treated mice in vivo. A recent study has shown that PDI physically interacts with $\alpha_v\beta_3$ integrin and that these two proteins co-localize at the surface of the activated endothelial cells (ECs) (Swiatkowska et al. 2008). Interaction between $\alpha_v\beta_3$ integrin and the extracellular matrix is crucial for angiogenesis through the full activation of VEGFR-2 triggered by VEGF-A (Soldi et al. 1999). Moreover, the specific inhibition of PDI by bacitracin remarkably impairs the ability of ECs to form tubular structures (Tian et al. 2009). Indeed, we identified that intra-tumoral $\alpha_v\beta_3$ stained vessel formation was significantly suppressed by PDI inhibition with bacitracin in this study. Moreover, immunoprecipitation analysis using the tumor tissue lysates revealed that bacitracin decreased both PDI expression and the interaction between PDI and $\alpha_v\beta_3$ integrin. These findings suggest that bacitracin had an anti-angiogenic effect by suppressing the role of $\alpha_v\beta_3$ integrin in angiogenesis by inhibiting the formation of the PDI-$\alpha_v\beta_3$ integrin complex (Swiatkowska et al. 2008). Collectively, PDI inhibition could therapeutically be useful in reducing tumor survival through the dual mechanisms of augmenting ER stress and the anti-angiogenic effect.

This study demonstrated that the inhibition of hypoxia-iniducible PDI enhanced 3-BP-induced HCC cell apoptosis. Moreover, 3-BP and bacitracin were also found to act synergistically in mice bearing HCC tumors by augmenting the ER stress and anti-angiogenesis, which suggests that the inhibition of PDI in combination with the inhibition of hexokinase II treatment may therapeutically be useful in patients with large or infiltrative hypovascular HCCs, which are aggressively growing under a hypoxic environment.

Acknowledgments This study was supported by a grant (No. 0320100210) from Seoul National University Hospital Research Fund; by a grant of the Korea Healthcare Technology R&D Project, Ministry of Health and Welfare, Republic of Korea (A102065); and by a grant from the Liver Research Foundation of Korea. The authors thank Ms. Sung-Hee Lee and Ms. Soo-Mi Lee for their excellent technical assistance.

Conflict of interest The authors declare that they have no conflict of interest.

References

Beal SL (1984) Population pharmacokinetic data and parameter estimation based on their first two statistical moments. Drug Metab Rev 15(1–2):173–193

Briggs JN (1957) Staphylococcic pneumonia in infants and young children. Can Med Assoc J 76(4):269–272

Bustamante E, Morris HP, Pedersen PL (1981) Energy metabolism of tumor cells. Requirement for a form of hexokinase with a propensity for mitochondrial binding. J Biol Chem 256(16):8699–8704

Chignard N, Shang S, Wang H, Marrero J, Brechot C, Hanash S et al (2006) Cleavage of endoplasmic reticulum proteins in hepatocellular carcinoma: Detection of generated fragments in patient sera. Gastroenterology 130(7):2010–2022

Di Bisceglie AM, Rustgi VK, Hoofnagle JH, Dusheiko GM, Lotze MT (1988) NIH conference. Hepatocellular carcinoma. Ann Intern Med 108(3):390–401

Dickerhof N, Kleffmann T, Jack R, McCormick S (2011) Bacitracin inhibits the reductive activity of protein disulfide isomerase by disulfide bond formation with free cysteines in the substrate-binding domain. FEBS J

Drake CJ, Cheresh DA, Little CD (1995) An antagonist of integrin alpha v beta 3 prevents maturation of blood vessels during embryonic neovascularization. J Cell Sci 108(Pt 7):2655–2661

Feng Y, Tian ZM, Wan MX, Zheng ZB (2007) Protein profile of human hepatocarcinoma cell line SMMC-7721: identification and functional analysis. World J Gastroenterol 13(18):2608–2614

Ganapathy-Kanniappan S, Vali M, Kunjithapatham R, Buijs M, Syed LH, Rao PP et al (2010a) 3-bromopyruvate: a new targeted antiglycolytic agent and a promise for cancer therapy. Curr Pharm Biotechnol 11(5):510–517

Ganapathy-Kanniappan S, Geschwind JF, Kunjithapatham R, Buijs M, Syed LH, Rao PP et al (2010b) 3-Bromopyruvate induces endoplasmic reticulum stress, overcomes autophagy and causes apoptosis in human HCC cell lines. Anticancer Res 30(3):923–935

Goplen D, Wang J, Enger PO, Tysnes BB, Terzis AJ, Laerum OD et al (2006) Protein disulfide isomerase expression is related to the invasive properties of malignant glioma. Cancer Res 66(20):9895–9902

Graven KK, Molvar C, Roncarati JS, Klahn BD, Lowrey S, Farber HW (2002) Identification of protein disulfide isomerase as an endothelial hypoxic stress protein. Am J Physiol Lung Cell Mol Physiol 282(5):L996–L1003

Gwak GY, Yoon JH, Kim KM, Lee HS, Chung JW, Gores GJ (2005) Hypoxia stimulates proliferation of human hepatoma cells through the induction of hexokinase II expression. J Hepatol 42 (3):358–364

Jordan PA, Gibbins JM (2006) Extracellular disulfide exchange and the regulation of cellular function. Antioxid Redox Signal 8(3–4):312–324

Kim W, Yoon JH, Jeong JM, Cheon GJ, Lee TS, Yang JI et al (2007) Apoptosis-inducing antitumor efficacy of hexokinase II inhibitor in hepatocellular carcinoma. Mol Cancer Ther 6(9):2554–2562

Kim W, Yoon JH, Kim JR, Jang IJ, Bang YJ, Kim YJ et al (2009) Synergistic anti-tumor efficacy of lovastatin and protein kinase C-beta inhibitor in hepatocellular carcinoma. Canc Chemother Pharmacol 64(3):497–507

Ming LJ, Epperson JD (2002) Metal binding and structure-activity relationship of the metalloantibiotic peptide bacitracin. J Inorg Biochem 91(1):46–58

Moenner M, Pluquet O, Bouchecareilh M, Chevet E (2007) Integrated endoplasmic reticulum stress responses in cancer. Cancer Res 67 (22):10631–10634

Mori K (2000) Tripartite management of unfolded proteins in the endoplasmic reticulum. Cell 101(5):451–454

Parkin DM, Pisani P, Ferlay J (1999) Estimates of the worldwide incidence of 25 major cancers in 1990. Int J Cancer 80 (6):827–841

Pastorekova S, Zatovicova M, Pastorek J (2008) Cancer-associated carbonic anhydrases and their inhibition. Curr Pharm Des 14 (7):685–698

Puig A, Lyles MM, Noiva R, Gilbert HF (1994) The role of the thiol/disulfide centers and peptide binding site in the chaperone and anti-chaperone activities of protein disulfide isomerase. J Biol Chem 269(29):19128–19135

Rapisarda A, Melillo G (2009) Role of the hypoxic tumor microenvironment in the resistance to anti-angiogenic therapies. Drug Resist Updates 12(3):74–80

Ron D, Walter P (2007) Signal integration in the endoplasmic reticulum unfolded protein response. Nat Rev Mol Cell Biol 8(7):519–529

Roth RA (1981) Bacitracin: an inhibitor of the insulin degrading activity of glutathione-insulin transhydrogenase. Biochem Biophys Res Commun 98(2):431–438

Soldi R, Mitola S, Strasly M, Defilippi P, Tarone G, Bussolino F (1999) Role of alphavbeta3 integrin in the activation of vascular endothelial growth factor receptor-2. EMBO J 18(4):882–892

Swiatkowska M, Szymanski J, Padula G, Cierniewski CS (2008) Interaction and functional association of protein disulfide isomerase with alphaVbeta3 integrin on endothelial cells. FEBS J 275(8):1813–1823

Szegezdi E, Logue SE, Gorman AM, Samali A (2006) Mediators of endoplasmic reticulum stress-induced apoptosis. EMBO Rep 7 (9):880–885

Tager M, Kroning H, Thiel U, Ansorge S (1997) Membrane-bound proteindisulfide isomerase (PDI) is involved in regulation of surface expression of thiols and drug sensitivity of B-CLL cells. Exp Hematol 25(7):601–607

Tezuka M, Hayashi K, Kubota K, Sekine S, Okada Y, Ina H et al (2007) Growth rate of locally recurrent hepatocellular carcinoma after transcatheter arterial chemoembolization: comparing the growth rate of locally recurrent tumor with that of primary hepatocellular carcinoma. Dig Dis Sci 52(3):783–788

Tian F, Zhou X, Wikstrom J, Karlsson H, Sjoland H, Gan LM et al (2009) Protein disulfide isomerase increases in myocardial endothelial cells in mice exposed to chronic hypoxia: a stimulatory role in angiogenesis. Am J Physiol Heart Circ Physiol 297(3):H1078–H1086

Trevisani F, Caraceni P, Bernardi M, D'Intino PE, Arienti V, Amorati P et al (1993) Gross pathologic types of hepatocellular carcinoma in Italian patients. Relationship with demographic, environmental, and clinical factors. Cancer 72(5):1557–1563

Weinstein-Oppenheimer CR, Henriquez-Roldan CF, Davis JM, Navolanic PM, Saleh OA, Steelman LS et al (2001) Role of the Raf signal transduction cascade in the in vitro resistance to the anticancer drug doxorubicin. Clin Cancer Res 7(9):2898–2907

Xu C, Bailly-Maitre B, Reed JC (2005) Endoplasmic reticulum stress: cell life and death decisions. J Clin Invest 115(10): 2656–2664

Yamashita YI, Shimada M, Hasegawa H, Minagawa R, Rikimaru T, Hamatsu T et al (2001) Electroporation-mediated interleukin-12 gene therapy for hepatocellular carcinoma in the mice model. Cancer Res 61(3):1005–1012

Yoon JH, Lee HS (2008) Experimental agents which inhibit hepatocarcinogenesis. Oncology 75(Suppl 1):17–21

Yu SJ, Yoon JH, Lee JH, Myung SJ, Jang ES, Kwak MS et al (2011) Inhibition of hypoxia-inducible carbonic anhydrase-IX enhances hexokinase II inhibitor-induced hepatocellular carcinoma cell apoptosis. Acta Pharmacol Sin 32(7):912–920

Zhou J, Zheng W, Cao L, Liu M, Han F, Li A (2010) Antiangiogenic tumor treatment: noninvasive monitoring with contrast pulse sequence imaging for contrast-enhanced grayscale ultrasound. Acad Radiol 17(5):646–651